Author/s:
Murphy, KT;Swiderski, K;Ryall, JG;Davey, JR;Qian, H;Lamon, S;Foletta, VC;Trieu, J;Chee, A;Read, SJ;Naim, T;Gregorevic, P;Lynch, GS

Title:
Mechanisms of chemotherapy‐induced muscle wasting in mice with cancer cachexia

Date:
2022-01

Citation:
Murphy, K. T., Swiderski, K., Ryall, J. G., Davey, J. R., Qian, H., Lamon, S., Foletta, V. C., Trieu, J., Chee, A., Read, S. J., Naim, T., Gregorevic, P. & Lynch, G. S. (2022). Mechanisms of chemotherapy‐induced muscle wasting in mice with cancer cachexia. JCSM Rapid Communications, 5 (1), pp.102-116. https://doi.org/10.1002/rco2.50.

Persistent Link:
https://hdl.handle.net/11343/289623

ORIGINAL ARTICLE

JCSM Rapid Communications (2021)
Published online in Wiley Online Library (wileyonlinelibrary.com) **DOI:** 10.1002/rco2.50

Mechanisms of chemotherapy-induced muscle wasting in mice with cancer cachexia

Kate T. Murphy[1]*, Kristy Swiderski[1], James G. Ryall[1], Jonathan R. Davey[1], Hongwei Qian[1], Séverine Lamon[2], Victoria C. Foletta[2], Jennifer Trieu[1], Annabel Chee[1], Suzannah J. Read[1], Timur Naim[1], Paul Gregorevic[1] & Gordon S. Lynch[1]

[1]*Centre for Muscle Research, Department of Anatomy and Physiology, The University of Melbourne, Melbourne, Victoria, Australia,* [2]*Institute for Physical Activity and Nutrition (IPAN), School of Exercise and Nutrition Sciences, Deakin University, Burwood, Victoria, Australia*

Abstract

Background Cachexia is a debilitating complication of cancer characterized by progressive wasting and weakness of skeletal muscles that reduces quality of life and can compromise survival. Many anticancer treatments, such as chemotherapy, also cause muscle wasting, which impairs the response to treatment. Given that many cancer patients present with cachexia at the initiation of treatment, we investigated whether cachectic mice were susceptible to chemotherapy-induced muscle wasting and to investigate contributing mechanisms, including the dysregulation of microRNAs (miRs).

Methods Cachectic colon-26 (C-26) tumour-bearing mice were given 5-fluourouracil (5-FU) chemotherapy or vehicle treatment and analysed for muscle mass, fibre size and composition, and miR expression. Mechanisms were validated *in vitro* using C2C12 cell culture and miR mimics and inhibitors and were confirmed *in vivo* by injecting muscles of 5-FU-treated cachectic mice with recombinant adeno-associated viral (rAAV) vectors encoding a miR sponge.

Results In cachectic tumour-bearing mice, 5-FU chemotherapy exacerbated the loss of skeletal muscle mass compared with vehicle treatment (by −12% to −20%, $P < 0.05$). miR expression profiling, quantitative real-time PCR, and *in vitro* analyses revealed contributing mechanisms including miR-351-3p-dependent ERK2 inhibition. Intramuscular injection of rAAV vectors encoding a sponge to reduce miR-351-3p expression in 5-FU-treated cachectic mice enhanced ERK phosphorylation (+18%, $P < 0.05$) and increased muscle fibre size (+15%, $P < 0.01$). Hsa-miR-125a-3p shares similar predicted gene targets as mmu-miR-351-3p, and its inhibition in human muscle cells *in vitro* prevented 5-FU-induced atrophy ($P < 0.001$) and increased ERK phosphorylation ($P < 0.001$).

Conclusions The findings implicate miR-351-3p-mediated ERK2 inhibition as a contributing mechanism in chemotherapy-induced muscle wasting in mice with cancer cachexia and that its inhibition is a promising adjunct therapy for preserving muscles during cancer treatment.

Keywords ERK2; miR-351; Chemotherapy; Cancer cachexia; Muscle wasting

Received: 21 February 2021; Revised: 21 June 2021; Accepted: 27 July 2021
**Correspondence to: Kate T. Murphy, Centre for Muscle Research, Department of Anatomy and Physiology, The University of Melbourne, Melbourne, Victoria 3010, Australia. Fax: +61 3 8344 5818, Email: ktmurphy@unimelb.edu.au*

Introduction

Cachexia is the profound weight loss, frailty, and fatigue that affects many cancer patients. It is a multifactorial syndrome that manifests as progressive wasting of skeletal muscle (and typically fat) and is associated with significant functional impairments.[1] In the worst cases, cachexia leads to metabolic, respiratory (diaphragm), and/or cardiac (heart) muscle failure and accounts for 20–30% of all cancer-related deaths.[2,3] Indeed, weight loss and body mass index are

predictors of survival in cancer patients.[4,5] Cachexia affects 40–80% of all advanced cancer patients with the highest prevalence in those with pancreatic, gastric, oesophageal, colorectal, and lung cancer.[6,7] It can also occur early in disease with weight loss present at diagnosis in >40% of patients with head and neck, gastrointestinal, pancreatic, colorectal, and lung cancers and is associated with reduced response to chemotherapy, increased treatment toxicity, and poorer survival.[8–11]

Anticancer treatments, such as chemotherapy, can also cause muscle wasting and weakness, with fatigue being one of the most debilitating side effects.[12] In patients, cachexia that develops during chemotherapy is associated with poor prognosis.[13] Preclinical studies in non-tumour-bearing mice have revealed that muscle wasting and weakness caused by 5-fluorouracil (5-FU)-based chemotherapy combinations result from muscle fibre atrophy, a shift from slow-to-fast fibre types, and mitochondrial dysfunction.[14,15] Furthermore, muscle wasting persisted in the colon-26 (C-26) mouse model of cancer cachexia despite cisplatin chemotherapy reducing tumour size by nearly four-fold.[16] Whether existing cachexia alters the effects of chemotherapy on skeletal muscle is unknown, but because many cancer patients present with cachexia when chemotherapy begins,[8–11] it is essential to determine whether they remain susceptible to chemotherapy-induced muscle wasting and, if so, to identify the mechanisms responsible. To this end, we focused mechanisms on dysregulated microRNAs (miRs) because they are important contributing regulators of muscle size[17] and protein turnover,[18] altered miR expression is associated with cancer cachexia[19–21] and other conditions of muscle wasting,[22,23] and miR-based therapies are effective and safe to use *in vivo*.[24] We tested the hypothesis that mice with cancer cachexia would remain susceptible to chemotherapy-induced muscle wasting as a consequence of dysregulated miR expression. This information has important implications for the design of adjuvant therapies and the development of strategies that can attenuate chemotherapy-induced muscle wasting, reduce the risk of recurrence, and improve survival for cancer patients.

Materials and methods

Experimental animals

All experiments were approved by the Animal Ethics Committee of The University of Melbourne and conducted in accordance with the Australian Code of Practice for the Care and Use of Animals for Scientific Purposes as stipulated by the National Health and Medical Research Council (Australia). Male CD2F1 and Balb/c mice were obtained from the Animal Resources Centre (Canning Vale, Western Australia) and housed in the Biological Research Facility at The University of Melbourne under a 12:12 h light–dark cycle. Water and standard laboratory chow were available *ad libitum*, and consumption was recorded daily.

Effect of 5-fluorouracil chemotherapy in cachectic tumour-bearing mice

Frozen C-26 cells were kindly donated by Prof. Martha Belury (The Ohio State University, Columbus, OH, USA). We have previously described the procedures used to thaw and count the C-26 cells and have characterized the functional and metabolic impairments in mice injected with these cells in detail elsewhere.[25]

On the day of inoculation (Day 1), 11- to 12-week-old CD2F1 mice were allocated randomly into one of three experimental groups: a control group injected with phosphate-buffered saline (PBS) alone (n = 8); a C-26 tumour-bearing group treated with DMSO vehicle (n = 6); and a C-26 tumour-bearing group treated with 5-FU (n = 7). Mice were anaesthetized via an intraperitoneal (i.p.) injection of a mixture of ketamine (100 mg·kg^{-1}) and xylazine (10 mg·kg^{-1}; VM Supplies, Chelsea Heights, VIC, Australia), such that they were unresponsive to tactile stimuli. Mice were shaved on the dorsal side and given a subcutaneous (s.c.) injection of 5×10^5 C-26 cells suspended in 100 μL of sterilized PBS or 100 μL of sterilized PBS only (control). Mice recovered from anaesthesia on a heat pad and were given an s.c. injection of atipamezole (Antisedan; 1 mg·kg^{-1}; VM Supplies) to partially reverse the effects of xylazine and promote faster recovery from sedation. On Days 15, 18, and 21, lean body mass was assessed (EchoMRI™, Houston, TX, USA) and mice received an i.p. injection of either 60% DMSO vehicle (3.3 μL·g^{-1} body mass; Sigma-Aldrich, Castle Hill, NSW, Australia) or 5-FU diluted in 60% DMSO (100 mg·kg^{-1} body mass, 3.3 μL·g^{-1} body mass; Sigma-Aldrich). The 5-FU dose was based on that used previously to reduce C-26 tumour size[26] and predicted to be within the clinical range (50–154 mg·kg^{-1} lean body mass).[27] On Day 22, mice were anaesthetized with sodium pentobarbitone (Nembutal; 60 mg·kg^{-1}; Sigma-Aldrich) via i.p. injection and various hindlimb skeletal muscles [tibialis anterior (TA), extensor digitorum longus, soleus, and plantaris] as well as the epididymal fat, spleen, heart, and tumour were carefully excised, blotted on filter paper, and weighed on an analytical balance. The TA muscles were mounted in embedding medium and frozen in thawing isopentane, and the other tissues were frozen rapidly in liquid nitrogen. All tissues were then stored at −80°C for subsequent analyses. Mice were killed as a consequence of heart excision while still anaesthetized deeply.

DOI: 10.1002/rco2.50

Generation and intramuscular injection of rAAV6:eGFP-miR-351-3p sponge in 5-FU-treated mice with cancer cachexia

Methods for the design, cloning, and *in vitro* validation of the AAV:eGFP-miR-351-3p sponge and scrambled controls are provided in the Supporting Information. Transfection of the AAV:eGFP-miR-351-3p sponge and AAV:eGFP-Scrambled control plasmids with the pDGM6 packaging plasmid into HEK 293 cells generated type 6 pseudotyped viral vectors that were harvested and purified as described previously.[28] Briefly, HEK 293 cells were plated on a 10 cm culture dish, 8–16 h prior to transfection with 10 μg of a vector genome-containing plasmid and 20 μg of the packaging plasmid pDGM6, using the calcium phosphate precipitate method to generate pseudotype 6 vectors. Seventy-two hours after transfection, the media and cells were collected and homogenized through a microfluidizer (Microfluidics) prior to 0.22 μm clarification (Millipore). Purified vector was generated from the clarified lysate by affinity chromatography over a HiTrap heparin column (Amersham) and ultracentrifuged overnight prior to resuspension in sterile Hank's balanced salt solution.

For this experiment, we used the more readily available Balb/c mouse model that has an endpoint of 18 days after the injection of C-26 cells, at which time mice exhibit a similar percentage decrease in tumour-free body mass and loss of muscle and heart mass as C-26 tumour-bearing CD2F1 mice at endpoint (21 days after C-26 injection). On the day of inoculation (Day 1), 15- to 16-week-old male Balb/c mice (n = 8) were anaesthetized with isoflurane (induction, 3–4% oxygen–isoflurane at 0.5 L·min^{-1}; maintenance, 2–3% at 0.5 L·min^{-1}), such that they were unresponsive to tactile stimuli. They were then shaved on the dorsal side and given an s.c. injection of 5×10^5 C-26 cells suspended in 100 μL of sterilized PBS. Four days later (Day 5), mice were again anaesthetized with isoflurane, both hindlimbs shaved and the right TA muscle was injected with rAAV6:eGFP-miR-351-3p sponge while the left TA muscle was injected with rAAV6:eGFP-Scrambled sponge at a dose of 5×10^9 vector genomes (determined by optimization pilot studies) in 40 μL of sterilized Hank's balanced salt solution. Mice were given an s.c. injection of buprenorphine (0.05 mg·kg^{-1}) for analgesia and recovered on a heat pad. To match the timing of 5-FU treatments to the CD2F1 model where injections were given every 3 days with the final injection given the day before endpoint, on Days 12, 15, and 18, mice received an i.p. injection of 5-FU diluted in 60% DMSO (100 mg·kg^{-1} body mass). On Day 19, mice were anaesthetized with sodium pentobarbitone (Nembutal; 60 mg·kg^{-1}) via i.p. injection and the right TA and left TA muscles were carefully excised, blotted on filter paper, and weighed on an analytical balance. The TA muscles were mounted in embedding medium, frozen in thawing isopentane, and stored at −80°C for subsequent analyses. Mice were killed by cardiac excision while still anaesthetized deeply.

Culture, transfection, and treatment of C2C12 cells

Murine C2C12 myoblasts (American Type Culture Collection, Manassas, VA, USA) were seeded in 12-well plates and cultured in growth media containing Dulbecco's modified Eagle's medium (DMEM, Life Technologies, Scoresby, VIC, Australia) supplemented with 10% FBS and 1% L-glut (DMEM/10% FBS/1% L-glut) at 37°C + 5% CO_2. Upon confluency, the media were changed to DMEM containing 2% (v/v) horse serum (HS, Life Technologies) and 1% L-glut (DMEM/2% HS/1% L-glut, differentiation media) for 4 days to induce differentiation during which time the media were changed every 48 h. For experiments assessing the effect of treatment with various chemotherapeutics, and as per our standard procedures,[29,30] treatment was initiated on Day 4 of differentiation, at which point we observe fully differentiated myotubes. Cells were then incubated for an additional 48 h at 37°C + 5% CO_2 in fresh DMEM/2% HS/1% L-glut containing 5-FU (5 μM in 0.0013% DMSO) or vehicle (0.0013% DMSO). Pilot dose–response experiments showed that 5 μM was the lowest dose of 5-FU to induce significant and reproducible atrophy.

For miRNA mimic and inhibitor experiments, murine C2C12 myoblasts were seeded in six-well plates and cultured in growth media at 37°C + 5% CO_2. When myoblasts reached ~75% confluency, they were transfected with 25 pmol of miRNA mimic negative control [Applied Biological Materials Inc. (ABM), Richmond, BC, Canada]; mmu-miR-351-3p mimic (ABM); miRNA inhibitor negative control (ABM); or mmu-miR-351-3p inhibitor (ABM) using Lipofectamine RNAiMAX Transfection Reagent (Invitrogen, Carlsbad, CA, USA), according to manufacturer's instructions. At 24 h after transfection, growth media were changed. At 48 h after transfection, the media were changed to differentiation media for 6 days, with media refreshed every 48 h. In these experiments, myotubes were incubated at 37°C + 5% CO_2 for 48 h (Days 4–6) in fresh differentiation media with vehicle control (0.0013% DMSO) or 5-FU (5 μM); vehicle control (0.2% DMSO), oxaliplatin (40 μM, Sigma-Aldrich), or cisplatin (50 μM, Sigma-Aldrich); and leucovorin (10 μg·ml^{-1}, Sigma-Aldrich) or irinotecan (20 μg·ml^{-1}, Sigma-Aldrich).

Statistics

All values are expressed as mean ± SEM unless stated otherwise. Groups were compared using Student's t-test or a one-way or two-way ANOVA, where appropriate. Bonferonni's *post hoc* test was used to determine significant differences between individual groups. The level of significance was set at $P < 0.05$ for all comparisons except global miRNA expression profiling where cut-offs for significant changes were a fold-change >1.5 and a P value ≤0.01.

DOI: 10.1002/rco2.50

Figure 1 Cachectic mice are susceptible to chemotherapy-induced muscle wasting. (A) Schematic of experimental design showing means of relative total (including tumour mass) body mass (% initial). Grey bars represent days of vehicle (DMSO) or 5-FU treatment. At the end of the experimental period, tumours were excised and weighed, allowing for calculation of (B) relative tumour mass (normalized for body mass) and (C) absolute mass of various hindlimb muscles, including the extensor digitorum longus (EDL), tibialis anterior (TA), plantaris, and soleus, as well as the (D) heart. (E) Representative images of TA muscle cross-sections reacted for laminin (*red*) to indicate all muscle fibres and myosin IIa (N2.261, *green*) to indicate type IIa fibres. Because mouse TA muscles express very few type I fibres, those fibres not reacting with N2.261 (i.e. black fibres in the *merge*) were assumed to be of type IIx/b. Quantification of N2.261 and laminin based on reaction intensity facilitated determination of (F) the proportion of type IIa and type IIx/b fibres (non-reacting with N2.261), (G) average cross-sectional area (CSA) of the type IIa and type IIx/b fibres and all muscle fibres, and (H) histogram analysis of the distribution of fibre size in vehicle-treated and 5-FU-treated cachectic C-26 tumour-bearing mice (B–D, F–G, unpaired *t*-test; H, two-way ANOVA; $*P < 0.05$; $**P < 0.01$; $***P < 0.001$; n = 5–6, ±SEM). Scale bar, 50 μm.

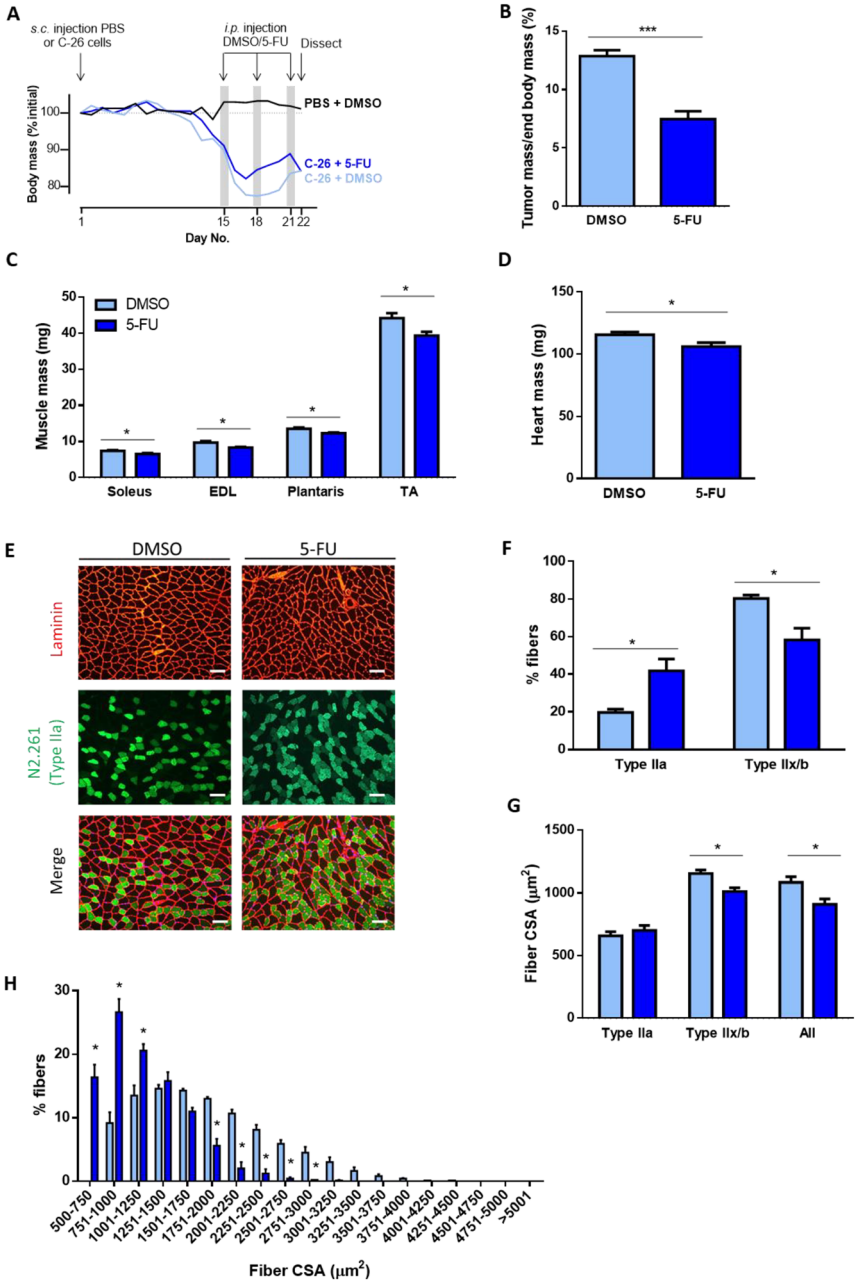

DOI: 10.1002/rco2.50

Further details about the Materials and methods section are provided in the Supporting Information.

Results

Cachectic mice are susceptible to chemotherapy-induced muscle wasting

As depicted in *Figure* 1A, cachectic CD2F1 mice bearing C-26 tumours received three intraperitoneal injections of vehicle (DMSO) or 5-FU (Days 15, 18, and 21) and, 1 day after the final injection, were anaesthetized deeply, and the tumour, various skeletal muscles, and organs were carefully excised and weighed. Lean body mass was assessed prior to each treatment, and calculations revealed that mice received an average 5-FU dose of 117 ± 2 $mg \cdot kg^{-1}$ lean body mass. No signs of 5-FU-related toxicity such as diarrhoea, palmar plantar erythematosus, mucositis, or ataxia were observed. Cumulative food intake was not different between vehicle-treated and 5-FU-treated mice (*Figure* S1A), but 5-FU increased cumulative water intake from Day 16 ($P < 0.0001$; *Figure* S1B). 5-FU had no effect on the percentage change in tumour-free body mass from the start of the experiment (*Figure* S1C) but reduced relative tumour mass by 42% compared with vehicle ($P < 0.001$, *Figure* 1B). Compared with vehicle, 5-FU treatment reduced mass of the soleus (by −13%, $P < 0.01$), extensor digitorum longus (by −14%, $P < 0.05$), plantaris (by −9%, $P < 0.05$), TA (by −11%, $P < 0.05$, all *Figure* 1C), and heart (by −8%, $P < 0.03$, *Figure* 1D) but had no effect on mass of the epididymal fat or spleen (*Figure* S1D).

Tibialis anterior muscle cross-sections were reacted for myosin IIa (N2.261, *green*) and laminin (*red*) to identify type IIa fibres and to visualize all fibres (*Figure* 1E), respectively, for assessment of fibre-type proportions and cross-sectional area. Because mouse TA muscles contain very few detectable type I fibres,[31] those fibres not reacting to N2.261 were assumed to be type IIx/b fibres. 5-FU induced a fibre-type shift towards more type IIa fibres (+22%, $P < 0.05$) and fewer type IIx/b fibres (−22%, $P < 0.05$, *Figure* 1F) and reduced cross-sectional area of the type IIx/b fibres (−15%, $P < 0.05$) and average of all muscle fibres compared with vehicle-treated controls (−16%, $P < 0.05$, *Figure* 1G). A histogram analysis confirmed that 5-FU reduced the proportion of larger muscle fibres and increased the proportion of smaller muscle fibres in cachectic mice ($P < 0.05$, *Figure* 1H).

Chemotherapy-induced muscle wasting is associated with miR-351-3p-dependent ERK2 inhibition

Given that recent studies have demonstrated that cancer cachexia is associated with dysregulated miR-regulated networks,[20,32,33] we performed global miR expression profiling analysis to identify whether miR expression alters with chemotherapy-induced wasting in cachectic mice. Of the 641 miRNAs measured, 313 (49%) were considered not expressed in mouse plantaris muscle and were therefore excluded from further analysis. Using a cut-off for significant changes of a fold-change >1.5 and P value ≤0.01 (q value <0.05), five miRs were differentially expressed (three up-regulated and two down-regulated) in plantaris muscles from 5-FU-treated mice compared with DMSO vehicle-treated mice (*Figure* 2A). Of the five differentially regulated miRs, only miR-351-3p was significantly increased with 5-FU when analysed by quantitative real-time PCR (qPCR, by 7.6-fold, $P < 0.05$, *Figure* 2B). Gene expression of the three up-regulated miRs was also examined in PBS mice and compared with DMSO vehicle-treated C-26 mice to differentiate between effects of cancer cells and chemotherapy. There were no differences between groups, indicating that the increase in miR-351-3p mRNA expression in 5-FU-treated cachectic mice was due to the chemotherapy and not the cancer cells (data not shown).

The gene targets of mouse miR-351-3p (mmu-miR-351-3p) were predicted on the basis of 3′UTR sequence homology, with 2370 potential targets identified, and these were submitted to KEGG analysis of signalling pathways (*Table* S1). Of known pathways typically associated with regulation of muscle size,[34] the MAPK signalling pathway was the top pathway enriched with predicted gene targets of mmu-miR-351-3p, including *Mapk1* (ERK2), *Mapk14* (p38), and *Mapk8* (JNK1) (*Figure* 2C and *Table* S1), and so we investigated the phosphorylation status of these proteins in muscles from vehicle-treated and 5-FU-treated cachectic mice (*Figure* 2D). 5-FU reduced ERK1/2 phosphorylation by 37% ($P < 0.05$) but had no effect on phosphorylation of p38 or p54/p46 SAPK/JNK (*Figure* 2E).

We used the C2C12 cell culture system to examine the direct effects of miR-351-3p modulation on myotube size and/or the phosphorylation status of ERK1/2. C2C12 myoblasts transfected with a miR-351-3p mimic and differentiated into mature myotubes resulted in a modest but significant increase in miR-351-3p expression (*Figure* 2F) and caused a 23% reduction in myotube size ($P < 0.0001$, *Figure* 2G) and a 43% decrease in ERK1/2 phosphorylation ($P < 0.05$, *Figure* 2H and 2I).

To further investigate the involvement of miR-351-3p in 5-FU-induced muscle atrophy, C2C12 myoblasts were transfected with a miR-351-3p inhibitor or negative control and, after 4 days of differentiation into myotubes, were treated for a further 48 h with 5-FU or vehicle control. The miR-351-3p inhibitor induced a trend for reduced miR-351-3p expression ($P < 0.06$, *Figure* 3A) and completely prevented atrophy induced by 5-FU ($P < 0.01$, *Figure* 3B). Furthermore, the miR-351-3p inhibitor prevented the 5-FU-induced decrease in ERK1/2 phosphorylation in C2C12

Figure 2 Increased miR-351-3p expression is associated with chemotherapy-induced muscle wasting in cachectic mice, and a miR-351-3p mimic induces myotube atrophy *in vitro*. (A) Comparative miRNA profiling analysis identified five miRNAs differentially expressed in plantaris muscles from 5-FU-treated cachectic mice compared with DMSO vehicle-treated cachectic mice (unpaired *t*-test; $^{**}P < 0.01$; $^{***}P < 0.001$; $^{****}P < 0.0001$; n = 4–5, ±SEM). (B) Quantitative real-time PCR (qPCR) analysis of the genes altered with miRNA profiling confirmed significant up-regulation of miR-351-3p in plantaris muscles from 5-FU-treated cachectic mice compared with DMSO vehicle-treated cachectic mice (unpaired *t*-test; $^{*}P < 0.05$; n = 4–6, ±SEM). (C) KEGG pathways enriched with predicted gene targets of mmu-miR-351-3p. Values next to the bars represent the number of enriched genes. (D, E) Western blot analysis of phosphorylated and total ERK1/2, p38 and p54/p46 SAPK/JNK, and total protein in plantaris muscles from DMSO vehicle-treated and 5-FU-treated cachectic mice (unpaired *t*-test; $^{*}P < 0.05$; n = 5–6, ±SEM). C2C12 myoblasts were transfected with a miRNA mimic negative control (-ve control) or miR-351-3p mimic and, after 6 days of differentiation, were taken for (F) qPCR analysis of miR-351-3p expression, (G) myosin and DAPI staining (*top*) to enable quantification of myotube diameter (*bottom*), and (H, I) western blot analysis of phosphorylated and total ERK1/2 and total protein (unpaired *t*-test; $^{*}P < 0.05$; $^{****}P < 0.0001$; E, n = 5; F, n = 5; G, n = 9–10; I, n = 4, ±SEM).

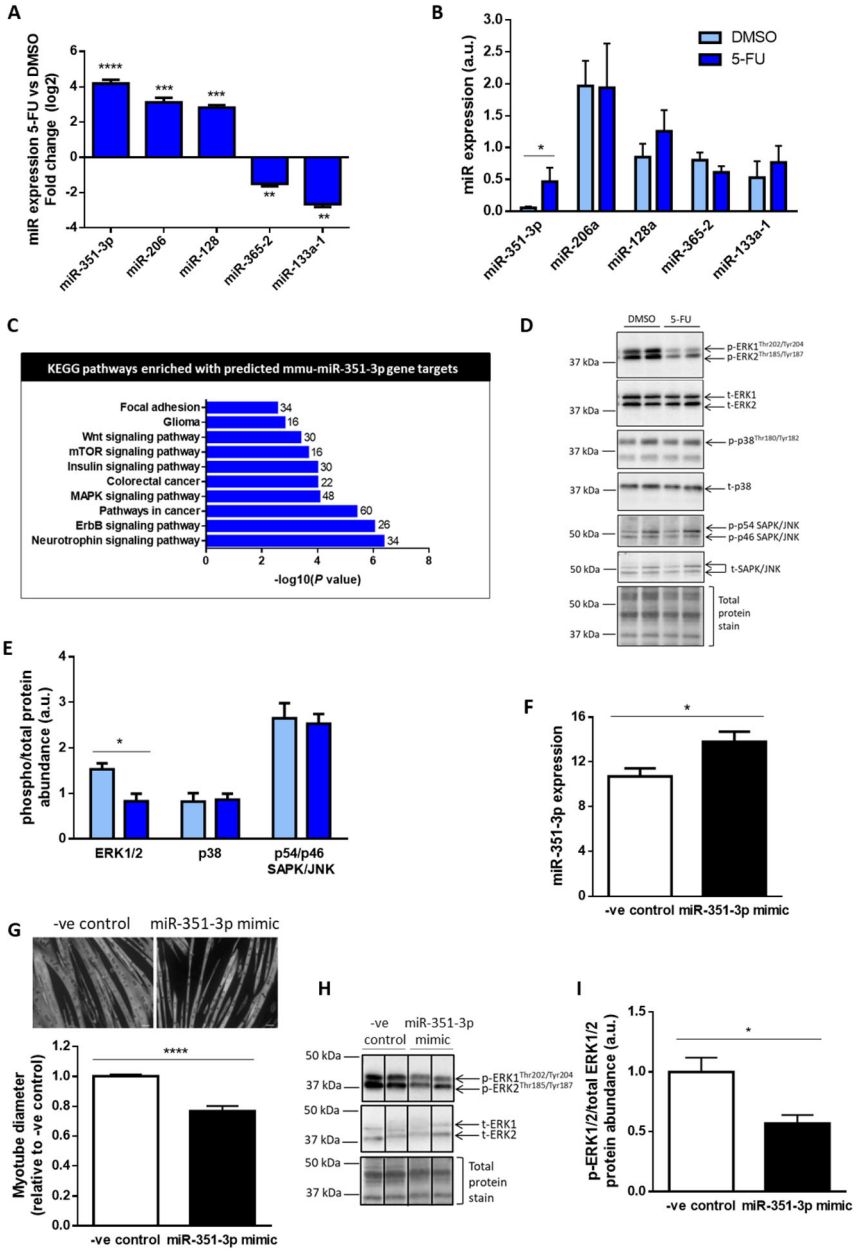

myotubes ($P < 0.05$, *Figure* 3C and 3D). To assess whether the findings reflected effects on proliferation, raw cell counts were taken at 24, 48, and 72 h after transfection and revealed very similar growth curves for C2C12 myoblasts transfected with the miR-351-3p inhibitor and inhibitor negative control (*Figure* S2A and S2B) and no difference between groups for

DOI: 10.1002/rco2.50

the mean doubling time (*Figure* S2C). These findings demonstrate that miR-351 inhibition does not affect the proliferative capacity of C2C12 myoblasts.

Given that the MAPK pathway has been associated with increased expression of the ubiquitin ligases MuRF-1 and atrogin-1, their expression was investigated in the experiments described previously. There was no difference in MuRF-1 ($P < 0.44$) or atrogin-1 mRNA expression ($P < 0.48$) in muscles from vehicle-treated and 5-FU-treated cachectic mice (*Figure* S2D). There was also no effect on MuRF-1 and atrogin-1 mRNA expression of the miR-351-3p mimic (*Figure* S2E) or of either 5-FU or the miR-351-3p inhibitor (*Figure* S2F).

To determine whether miR-351-3p could directly bind and regulate the *Mapk1* 3′UTR, HEK 293 cells were co-transfected with a reporter plasmid containing the full-length mouse

Figure 3 miR-351-3p inhibition prevents 5-FU-induced reductions in myotube size and ERK1/2 phosphorylation, and *Mapk1* (ERK2) is a direct target gene of miR-351-3p. C2C12 myoblasts were transfected with a miRNA inhibitor negative control (-ve control) or miR-351-3p inhibitor and, (A) after 6 days of differentiation into myotubes, were assessed for miR-351-3p expression using qPCR or, after 4 days of differentiation into myotubes, were treated for another 48 h with DMSO vehicle or 5-FU and then taken for (B) myosin and DAPI staining (*left*) for quantification of myotube diameter (*right*) or (C, D) western blot analysis of phosphorylated and total ERK1/2 and total protein (A, unpaired *t*-test; B & D, two-way ANOVA; $^{*}P < 0.05$; $^{**}P < 0.01$; $^{\#}P < 0.06$; A, $n = 6$; B, $n = 6$–9; D, $n = 6$–10, ±SEM). (E) NanoLuc luciferase activity was assessed in HEK 293 cells after co-transfection with 150 ng pNanoglo2 vector containing the full-length *Mapk1* 3′UTR and either 5 nM miR-351-3p mimic (+) or 5 nM of an irrelevant miRNA (negative control, −) (unpaired *t*-test; $^{***}P < 0.001$, experiment conducted three times using $n = 6$ wells per group, ±SEM). (F) *Top*, schematic of the putative binding site between miR-351-3p and the *Mapk1* 3′UTR at position 1426 (WT, blue font). *Bottom*, NanoLuc luciferase activity was assessed in HEK 293 cells following co-transfection with 150 ng pNanoglo2 vector containing either the putative miR-351-3p binding site of *Mapk1* 3′UTR (WT) or its mutant control and either 5 nM miR-351-3p mimic (+) or 5 nM of an irrelevant miRNA (negative control, −) (two-way ANOVA; $^{****}P < 0.0001$, experiments repeated three times using $n = 6$ wells per group, ±SEM).

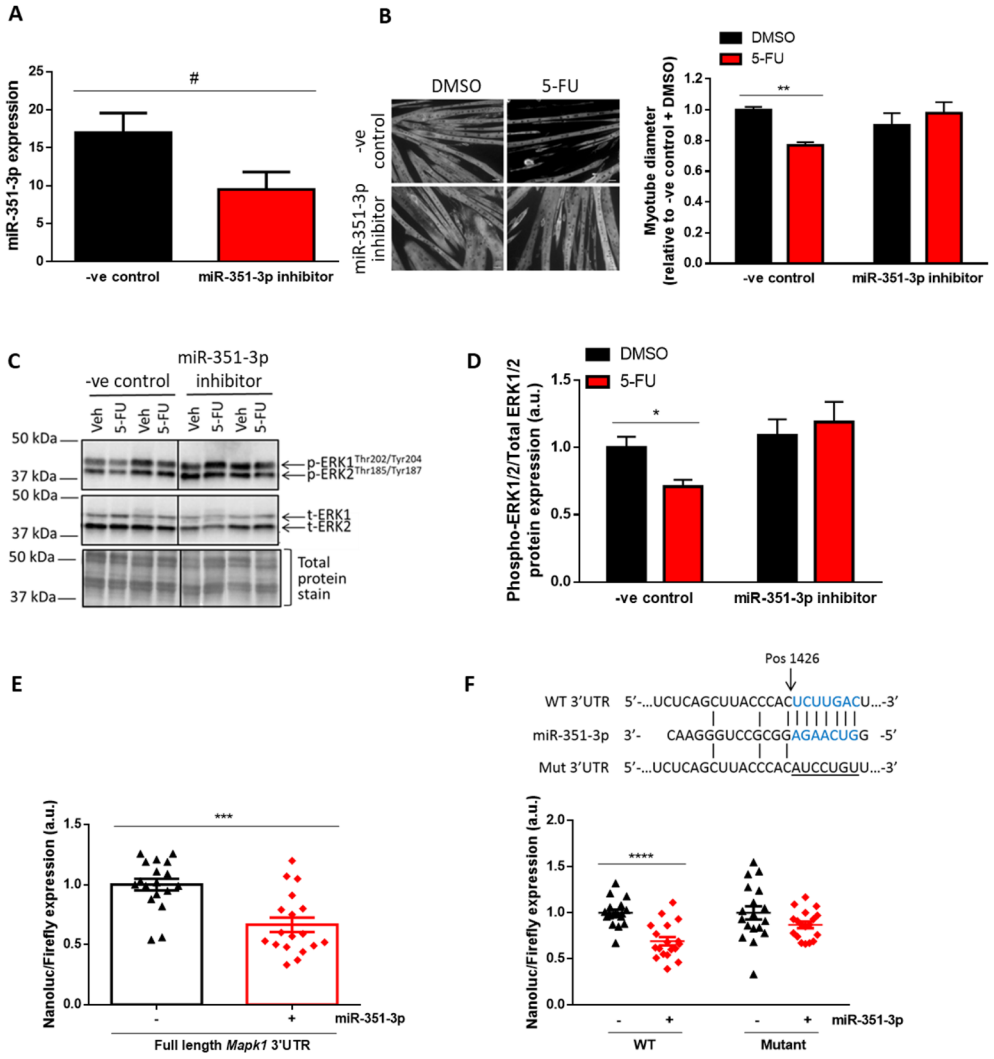

DOI: 10.1002/rco2.50

Mapk1 3′UTR alongside either a miR-351-3p mimic or an irrelevant miRNA lacking the predicted binding site on the *Mapk1* 3′UTR (negative control). HEK 293 cells were used for this purpose due to their high transfection efficiency. At 24 h after co-transfection, there was a 33% reduction in luciferase activity in the cells containing the miR-351-3p mimic compared with the negative control ($P < 0.001$, *Figure* 3E). We then investigated the miR-351-3p putative binding site on the *Mapk1* 3′UTR by co-transfecting HEK 293 cells with the miR-351-3p mimic or negative control as well as a reporter plasmid with a shorter version of the *Mapk1* 3′UTR containing only the putative miR-351-3p binding site (WT, *Figure* 3F). At 24 h after co-transfection, there was a 31% reduction in luciferase activity ($P < 0.0001$) in cells containing the miR-351-3p mimic compared with the negative control (*Figure* 3F). However, this reduction was completely prevented when cells were co-transfected with a shorter *Mapk1* 3′UTR reporter plasmid in which the miR-351-3p binding site was mutated (Mut, $P < 0.13$, *Figure* 3F). Taken together, these data indicate that *Mapk1* is a direct target of miR-351-3p.

miR-351-3p inhibition increases muscle fibre size in chemotherapy-treated cachectic mice

To test the therapeutic potential of miR-351-3p inhibition for attenuating chemotherapy-induced muscle fibre atrophy, we generated a AAV:eGFP-miR-351-3p sponge (*Figure* S3A) and AAV:eGFP-Scrambled (control) sponge plasmid. Function of the AAV:eGFP-miR-351-3p sponge was confirmed with transduction of C2C12 myotubes preventing the 5-FU-associated decrease in myotube size observed with the scrambled sponge (−26%, $P < 0.0001$; *Figure* S3B). These findings also confirm that effects of the miR-351-3p inhibitor were directly on myotubes and not myoblasts.

Having confirmed the function of the vector *in vitro*, we generated AAV6 preparations to test whether AAV6-mediated inhibition of miR-351-3p expression could increase muscle fibre size in 5-FU-treated mice with cancer cachexia. For this experiment, we used the more readily available Balb/c mouse model, which, after the injection of C-26 cells, develops tumours at a similar rate and size as the CD2F1 model (*Figure* S3C) and, at endpoint (Day 19), exhibits a similar percentage decrease in tumour-free body mass (*Figure* S3D) and loss of muscle and heart mass as C-26 tumour-bearing CD2F1 mice (*Figure* S3E). A schematic of the experimental timeline is shown in *Figure* 4A, with intramuscular injection of AAV6 on Day 5 (4 days after C-26 injection) and 5-FU treatments on Days 12, 15, and 18 to match the timing in the CD2F1 model where injections occurred every 3 days with the final injection given the day before endpoint. At 14 days after intramuscular injection into the TA muscles of cachectic C-26 tumour-bearing mice (Day 19), western blotting for GFP confirmed effective transduction of AAV6:eGFP-Scrambled sponge and AAV6:eGFP-miR-351-3p sponge vectors (*Figure* 4B), and injection of the AAV6:eGFP-miR-351-3p sponge increased ERK1/2 phosphorylation (+18%, $P < 0.05$, *Figure* 4B and 4C). H&E staining revealed no evidence of toxicity after intramuscular injection of AAV6:eGFP-miR-351-3p sponge or AAV6:eGFP-Scrambled control sponge (*Figure* 4D). Immunohistochemistry was used to differentiate between transduced (GFP positive) and non-transduced (GFP negative) fibres and revealed that the average size of fibres transduced with the AAV6:eGFP-miR-351-3p sponge was greater than those transduced with AAV6:eGFP-Scrambled sponge (+15%, $P < 0.01$, *Figure* 4E and 4F), due to a reduced proportion of smaller muscle fibres and an increased proportion of larger muscle fibres ($P < 0.05$, *Figure* 4G). qPCR was performed to examine changes in expression of the myosin heavy chain (MHC) isoforms and found an increase in MHCIIb mRNA expression (+130%, $P = 0.05$, *Figure* 4H) but no change in MHCIIa or MHCIIx mRNA expression with the AAV6:eGFP-miR-351-3p sponge.

Relevance to other chemotherapeutic drugs and human cancer

To gain a better understanding of the therapeutic potential of miR-351-3p inhibition, we examined the ability of the miR-351-3p inhibitor to attenuate muscle wasting in response to other chemotherapeutic agents. These included leucovorin and oxaliplatin, which are often used in combination with 5-FU (Folfox) as well as irinotecan, used in combination with 5-FU and leucovorin (Folfiri). Cisplatin was also examined as it is used to treat numerous human cancers including lung, ovarian, breast, bladder, head and neck, and testicular cancer. None of the chemotherapeutic agents increased endogenous miR-351-3p mRNA expression (*Figure* S4A and S4B). When added to C2C12 myotubes *in vitro*, oxaliplatin and cisplatin reduced myotube size by 23% ($P < 0.0001$) and 28% ($P < 0.0001$), respectively; effects were completely prevented by miR-351-3p inhibition (*Figure* S4C and S4D). Irinotecan increased ERK1/2 phosphorylation (by 1.77-fold, $P < 0.01$), but neither leucovorin nor irinotecan induced C2C12 myotube atrophy (*Figure* S4E and S4F) and so were not combined with the miR-351-3p inhibitor. Thus, miR-351-3p inhibition may have broad therapeutic potential across multiple and specific chemotherapy regimens.

miR-351-3p is not expressed in the human genome, and so we sought to identify a human miRNA targeting similar genes and pathways. Using miRWalk software and KEGG pathway analysis, we found that 16 of the 27 pathways enriched in predicted gene targets of human miR-125a-3p (hsa-miR-125a-3p) were shared with mouse miR-351-3p (mmu-miR-351-3p, *Table* S2). Furthermore, the MAPK signalling pathway was the top-ranked pathway enriched in genes

DOI: 10.1002/rco2.50

Figure 4 Intramuscular injection of AAV6:eGFP-miR-351-3p sponge increases muscle fibre size in chemotherapy-treated mice with cancer cachexia. (A) Experimental timeline showing that at 4 days (Day 5) after injection of C-26 cells, the right TA (RTA) muscles of Balb/c mice were injected with AAVs encoding for GFP-tagged miR-351-3p sponge and the left TA (LTA) muscles were injected with equivalent doses of GFP-tagged scrambled control sponge, and mice were given an i.p. injection of 5-FU on Days 12, 15, and 18. On Day 19, the RTA and LTA muscles were taken for western blot assessment of (B) GFP expression and (B, C) phosphorylated and total ERK1/2 expression. TA muscle sections were stained (or reacted for): (D) H&E to examine general muscle morphology and signs of toxicity and (E) wheat germ agglutinin (*red*) to indicate all muscle fibres and facilitate determination of (F) average CSA of the transduced fibres (GFP positive, *green*) and (G) histogram analysis of the size of transduced (GFP positive) fibres in muscles injected with AAV6:eGFP-Scrambled sponge (LTA) or AAV6:eGFP-miR-351-3p sponge (RTA) in 5-FU-treated cachectic mice. (H) qPCR analysis of the mRNA expression of MHCIIa, MHCIIb, and MHCIIx in muscles injected with AAV6:eGFP-Scrambled sponge or AAV6:eGFP-miR-351-3p sponge in 5-FU-treated cachectic mice. (C, F, H, unpaired *t*-test; G, two-way ANOVA; $*P < 0.05$; $**P < 0.01$; n = 6–8, ±SEM). Scale bar, 100 μm.

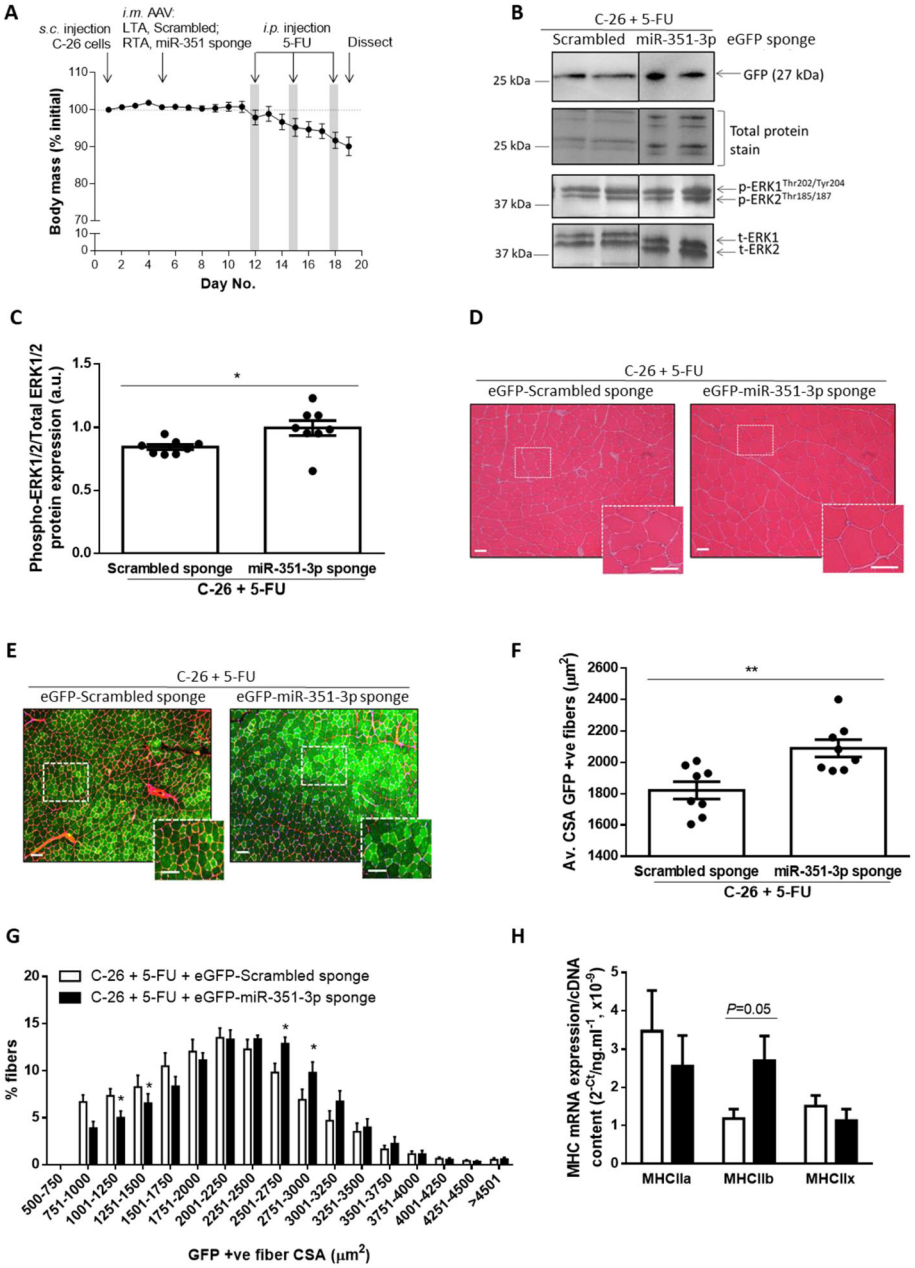

DOI: 10.1002/rco2.50

predicted to be targets of hsa-miR-125a-3p (*Figure* 5A and *Table* S2), including *MAPK1*, which contains four potential miR-125a-3p binding sites (*Figure* 5B). To assess the relevance of our findings to humans, we tested whether hsa-miR-125a-3p inhibition could attenuate 5-FU-induced atrophy of human primary skeletal muscle cells (*Figure* 5C and 5D). Transfection of the hsa-miR-125a-3p inhibitor had no effect on the size of DMSO-treated myotubes ($P < 0.69$) but completely prevented the 5-FU-induced reduction in muscle cell size and ERK1/2 phosphorylation ($P < 0.001$; *Figure* 5C and 5D). Therefore, inhibition of hsa-miR-125a-3p, which is predicted to target similar genes and pathways as mmu-miR-351a-3p, has therapeutic potential for attenuating chemotherapy-induced muscle wasting in patients with cancer cachexia.

Discussion

Given that many cancer patients present with cachexia at diagnosis and initiation of anticancer treatment, and because chemotherapy itself can cause muscle wasting and weakness, we investigated whether mice with existing cachexia were susceptible to chemotherapy-induced muscle wasting. Here, we show that in mice with cancer cachexia, 5-FU

Figure 5 miR-125a-3p targets similar genes and pathways as miR-351-3p, and inhibition of human miR-125a-3p prevents 5-FU-induced atrophy and reduction in ERK1/2 phosphorylation in human muscle cells *in vitro*. (A) Top-ranked KEGG pathways enriched with predicted gene targets of hsa-miR-125a-3p. Values next to the bars represent the number of predicted gene targets. (B) Human hsa-miR-125a-3p has four predicted binding sites to the human *Mapk1* 3′UTR. (C, D) Primary human skeletal muscle cells were transfected with a miRNA inhibitor negative control (-ve control) or hsa-miR-125a-3p inhibitor and, after 8 days of differentiation, were treated for 48 h with DMSO vehicle or 5-FU and then taken for (C) myosin and DAPI staining (*left*) for quantification of myotube diameter (*right*) or (D) western blot analysis of phosphorylated and total ERK1/2 (two-way ANOVA; $^{***}P < 0.001$; $n = 6$, ±SEM).

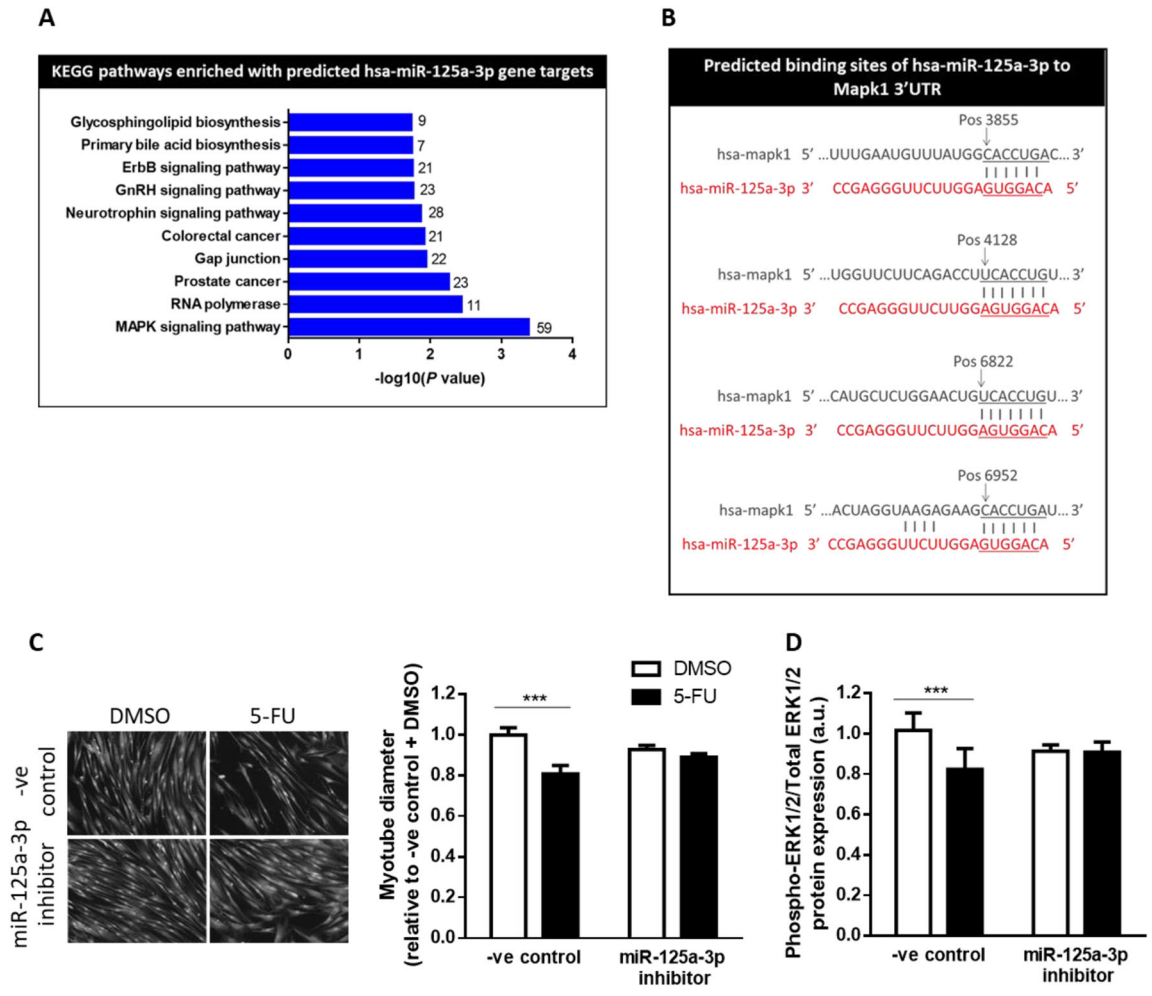

DOI: 10.1002/rco2.50

chemotherapy treatment increased loss of skeletal muscle and heart mass despite reducing tumour mass. As summarized in *Figure* 6, mechanisms mediating the chemotherapy-associated muscle wasting in cachectic mice include miR-351-3p-dependent ERK2 inhibition. Reducing miR-351-3p levels with an AAV-based sponge in skeletal muscle of 5-FU-treated mice with cancer cachexia enhanced ERK phosphorylation and increased muscle fibre size. These findings identify potential therapeutic targets and strategies to preserve muscle fibres during chemotherapy in patients with cancer cachexia.

Because more than 40% of patients with gastrointestinal, pancreatic, colorectal, and lung cancer exhibit cachexia upon diagnosis and the initiation of anticancer treatment,[8–11] it is clinically relevant to determine whether these patients are susceptible to chemotherapy-induced wasting and, if so, identify potential mechanisms and treatments to preserve skeletal muscle mass and quality of life in an already fragile population. We chose 5-FU-based chemotherapy as it is the common drug in combination therapies such as Folfox (5-FU, leucovorin, and oxaliplatin) and Folfiri (5-FU, leucovorin, and irinotecan) that are used frequently to treat cancers associated with early cachexia. Using 5-FU alone enables identification of its specific effects that could not be discerned with combination therapy. Importantly, the dose received normalized to lean body mass (~117 mg·kg^{-1}) was within the clinical range (50–154 mg·kg^{-1}).[27] We found that 5-FU treatment initiated after C-26 tumour-bearing mice had already began to exhibit cachexia exacerbated chemotherapy-induced wasting of skeletal muscles and the heart. Although cardiac function was not assessed in the present study, it is well known that chemotherapeutic agents cause cardiotoxic side effects,[35] with >20% of patients receiving 5-FU exhibiting cardiotoxicity.[36] The increased loss of heart mass in 5-FU-treated mice highlights the need for non-5-FU-based chemotherapeutics for cachectic patients in order to reduce toxic effects on the heart. Although 5-FU and other chemotherapeutics are frequently associated with anorexia, this was not observed in the present study, which is likely due to cachectic C-26 tumour-bearing mice already exhibiting anorexia compared with PBS controls.[25]

The mechanisms underlying chemotherapy-induced muscle wasting in cachectic mice remain largely unknown with most studies having been conducted in non-tumour-bearing rodents,[14,15,37–41] limiting their clinical relevance. The few studies comparing chemotherapy treatment in tumour-bearing and non-tumour-bearing mice have found that despite treatment inducing similar reductions in muscle mass, mechanisms vary considerably between groups.[16,42] It was therefore essential in the present study to investigate

Figure 6 In cachectic tumour-bearing mice, 5-FU-based chemotherapy induces miR-351-3p-mediated ERK2 inhibition in skeletal muscle, leading to increased wasting and poor prognosis. Inhibition of miR-351-3p using AAV-based gene therapy is a potential adjunct therapy for attenuating chemotherapy-induced muscle wasting and improving prognosis in cancer cachexia.

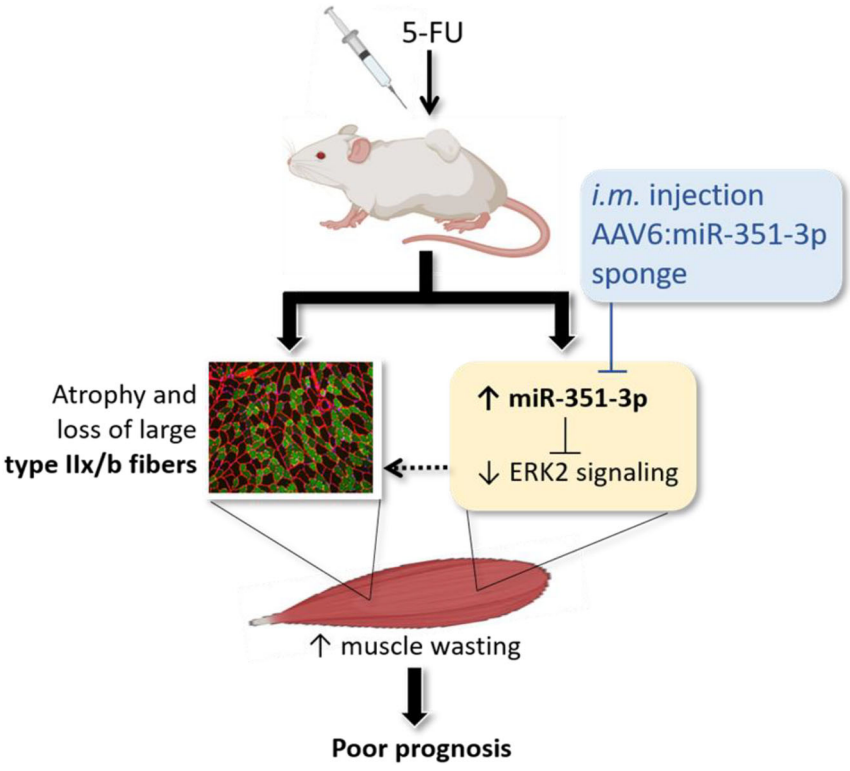

DOI: 10.1002/rco2.50

mechanisms underlying the susceptibility of cachectic muscles to chemotherapy-induced wasting, and in this regard, we focused on dysregulated miRs because they are important contributing regulators of muscle size,[17] altered miR expression is associated with numerous muscle wasting conditions[22,23] including cancer cachexia,[19–21] and miR-based therapies are effective and safe to use *in vivo*.[24] Global miR expression profiling and qPCR analyses revealed mechanisms of 5-FU-induced muscle wasting to include increased expression of miR-351-3p, and using luciferase reporter assays, we demonstrated that ERK2 is a direct gene target of miR-351-3p. Supporting these results, ERK1/2 phosphorylation was decreased in muscles from 5-FU-treated cachectic mice and associated with selective atrophy and loss of the large, glycolytic type IIx/b muscle fibres. These findings are consistent with previous reports of ERK1/2 inhibition inducing muscle atrophy[43] and a fibre-type shift.[44] However, they contrast with those implicating increased ERK1/2 phosphorylation in the pathophysiology of cachexia in tumour-bearing mice[45–47] and those in healthy mice where ERK1/2 activation was associated with Folfox- and Folfiri-induced muscle wasting.[15] The discrepancies provide further evidence that different mechanisms are responsible for chemotherapy-induced muscle wasting in tumour-bearing and non-tumour-bearing mice. They may also reflect effects of irinotecan, which increased ERK1/2 phosphorylation in the present study but did not induce C2C12 myotube atrophy. However, they are unlikely to involve effects of leucovorin (used in both Folfox and Folfiri), which did not affect myotube size or ERK1/2 phosphorylation.

This is the first report of miR-351-3p as a mediator of chemotherapy-induced wasting and adds to the growing body of evidence implicating dysregulated miR-regulated networks in cancer cachexia[20,32,33] and the regulation of skeletal muscle MAPK signalling.[48] There is a dearth of information on the role of miR-351-3p in skeletal muscle, but our *in vitro* experiments revealed that its overexpression reduced C2C12 myotube size and its inhibition did not alter the size of healthy myotubes but completely prevented myotube atrophy induced by chemotherapeutics including 5-FU, oxaliplatin, and cisplatin. Proliferation experiments confirmed that miR-351-3p inhibition did not affect C2C12 proliferation, and transduction of myotubes with an AAV:eGFP-miR-351-3p sponge confirmed direct effects on myotube size. Taken together, these findings suggest that endogenous miR-351-3p expression is low with little effect on the regulation of healthy muscle size but that its expression can increase significantly with some cytotoxic drugs such as 5-FU and contribute to muscle wasting in these conditions. Importantly, inhibition of miR-351-3p can also be beneficial for reducing the muscle wasting associated with other cytotoxic drugs such as oxaliplatin and cisplatin even without an increase in its endogenous expression.

We used intramuscular injection of an AAV-based therapeutic expressing a miRNA sponge to specifically inhibit miR-351-3p expression in a single skeletal muscle and investigate its therapeutic potential for protecting cachectic muscle from chemotherapy-induced wasting. Advantages of this system include that miRNA sponges are plasmid constructs containing multiple high-affinity miRNA antisense binding sites that can inhibit specific miRNAs and prevent their binding to endogenous target genes. Because of tissue limitations, we were unable to assess the unlikely possibility that other miRs were altered with the miR-351-3p sponge, but combining AAV with a tissue-specific promoter and a miRNA sponge limits regulation to a specific organ and avoids potential off-target effects typically associated with systemic delivery of miRNA sponges.[49] These benefits have enhanced the likelihood of vector-based strategies manipulating miRNA activity entering the clinic. Because we used a dose of AAV that reduces miR-351-3p levels without inducing toxicity and not transducing all muscle fibres, the addition of a GFP tag to the sponge constructs revealed that transduced (GFP-positive) fibres were significantly larger with the miR-351-3p sponge compared with the scrambled control sponge in 5-FU-treated cachectic mice. These findings demonstrate the utility of our approach for inhibiting miR-351-3p activity in striated muscle and provide proof-of-principle evidence of its therapeutic potential for protecting cachectic muscles from chemotherapy-induced wasting. A limitation of the constructs containing a GFP tag is that we were unable to assess whether the miR-351-3p sponge attenuated the 5-FU mediated fibre-type shift because the filter for immunohistochemical detection of GFP is the same as that for identification of the type IIa fibres. However, qPCR analysis of the mRNA expression of the MHC isoforms expressed in mouse TA muscles supported this notion by revealing that the miR-351-3p sponge increased MHCIIb expression.

Although miR-351-3p is not expressed in the human genome, we identified that human miR-125a-3p shares similar predicted target genes and pathways, including *MAPK1* (ERK2) and other members of the MAPK signalling pathway, and is part of the miR-125 family that has been implicated in carcinogenesis and chemoresistance.[50] Furthermore, miR-125a-3p inhibition completely prevents 5-FU-induced decreases in ERK1/2 phosphorylation and atrophy of primary human skeletal muscle cells, establishing the relevance of our findings to humans. Thus, local inhibition of miR-125a-3p could help prevent chemotherapy-induced wasting in patients with cancer cachexia. Further development of the viral vector approach for manipulating miRNA activity could include intravascular injection to achieve widespread transduction of striated musculature, including the heart, which exhibits susceptibility to 5-FU-induced wasting in cachectic mice.

In conclusion, mice with cancer cachexia remain susceptible to chemotherapy-induced muscle wasting, with

DOI: 10.1002/rco2.50

mechanisms including miR-351-3p-dependent ERK2 inhibition. We have identified inhibition of mmu-miR-351-3p/hsa-miR-125a-3p as a potential adjunct therapy for attenuating chemotherapy-induced muscle wasting in patients with cancer cachexia. These findings highlight the importance of initiating strategies to combat cachexia prior to treatment to enhance the effectiveness of chemotherapy and improve cancer prognosis.

Acknowledgements

The authors thank Prof. Martha Belury (Department of Human Nutrition, The Ohio State University) for donating the C-26 cells and Prof. Donna McCarthy (College of Nursing, The Ohio State University) for arranging the shipment of these cells, Dr Marissa Caldow (Centre for Muscle Research, Department of Anatomy and Physiology, The University of Melbourne) for donating the primary human skeletal muscle cells, and Associate Professor Peter Crack (Department of Biochemistry and Pharmacology, The University of Melbourne) for use of the FlexStation 3 machine. The MF 20 monoclonal antibody, developed by D. A. Fischman (Weill Cornell Medical College), and the N2.261 monoclonal antibody, developed by H. M. Blau (Standford University School of Medicine), were obtained from the Developmental Studies Hybridoma Bank, created by the NICHD of the NIH and maintained at The University of Iowa, Department of Biology, Iowa City, IA 52242.

Funding

This study was supported by project grants from the National Health and Medical Research Council (NHMRC, Australia, GNT1041865, to G.S.L. and K.T.M.), Victorian Cancer Agency (16852, to K.T.M.), and Cancer Council Victoria (1120752, to K.T.M. and G.S.L.). K.T.M. was supported by a Career Development Fellowship from the NHMRC (1023178). K.S. was supported by an Early Career Fellowship from the NHMRC (575580) and an Early Career Seed grant from The University of Melbourne.

Online supplementary material

Additional supporting information may be found online in the Supporting Information section at the end of the article.

Figure S1. (**A**) Cumulative food intake and (**B**) water intake in DMSO vehicle and 5-FU treated cachectic C-26 tumor-bearing CD2F1 mice. Grey bars represent days of DMSO or 5-FU treatment (two-way ANOVA; ****$P < 0.0001$; n = 5–7, ± SEM). At the end of the experimental period, (**C**) the percentage change in tumor-free body mass compared with initial (pre-inoculation) was calculated and (**D**) epididymal fat and spleen mass determined (unpaired *t*-test, no significant differences were found; n = 5–6, ± SEM).

Figure S2. To assess effects on proliferation, C2C12 myoblasts were transfected with a miRNA inhibitor negative control (-ve control) or miR-351-3p inhibitor and at 24, 48 and 72 h post-transfection, (**A**) representative bright field images were taken and (**B**) total cell counts were used to generate exponential growth curves and (**C**) mean doubling time (T_d; no significant differences were found; n = 4, mean ± SEM for B and mean ± 95% confidence interval for C). (**D**) qPCR analysis of MuRF-1 and atrogin-1 mRNA expression in plantaris muscles from 5-FU compared with DMSO vehicle treated cachectic mice (unpaired *t*-test; no significant differences were found; n = 5–6, ± SEM). (**E**) C2C12 myoblasts were transfected with a miRNA mimic negative control (-ve control) or miR-351-3p mimic and after 6 days of differentiation, were taken for qPCR analysis of MuRF-1 and atrogin-1 mRNA expression (unpaired *t*-test; no significant differences were found, n = 5, ± SEM). (**F**) C2C12 myoblasts were transfected with a miRNA inhibitor negative control (-ve control) or miR-351-3p inhibitor and after 4 d differentiation into myotubes, were treated for another 48 h with DMSO vehicle or 5-FU and then taken for qPCR analysis of MuRF-1 and atrogin-1 mRNA expression (two-way ANOVA; no significant differences were found, n = 6, ± SEM).

Figure S3. (**A**) Schematic showing design of the miR-351-3p sponge including four repeats of: two miR-351-3p binding sites (8 nt and 9 nt); a 3 nt bulge at nucleotide position 10–13; and 4 nt spacer sequence between the individual sponges, under the control of the CMV promoter. Inset shows nucleotide sequence of each sponge repeat (red) that sequesters the target miRNA (black). (**B**) C2C12 myotubes that had been differentiated for 1 d were transduced with a AAV:eGFP-Scrambled (control) sponge or AAV:eGFP-miR-351-3p sponge and after an additional 3 d differentiation, were treated for 48 h with DMSO vehicle or 5-FU and then taken for: (B) imaging of GFP to assess transduction efficiency (*left*) and then myosin and DAPI staining to enable quantification of myotube diameter (*right*, two-way ANOVA; ****$P < 0.0001$; n = 3, ± SEM). Comparison of (**C**) tumor growth, (**D**) the percentage change in tumor-free body mass from the start of the experiment to end-point (day 22 in CD2F1 model and day 19 in Balb/c model) and (**E**) the percentage change in mass of the extensor digitorum longus (EDL), tibialis anterior (TA) and heart compared with PBS controls in CD2F1 and Balb/c mice injected subcutaneously with C-26 cells (C, two-way ANOVA; D-E, unpaired *t*-test; no significant differences were found; n = 5–6, ± SEM).

Figure S4. C2C12 myotubes that had been differentiated for 4 d were treated for another 48 h with: (**A**) DMSO

vehicle (control), oxaliplatin or cisplatin; or (**B**) leucovorin or irinotecan and then taken for qPCR analysis of miR-351-3p mRNA expression (one-way ANOVA; no significant differences were found; n = 4, ± SEM). (**C**, **D**) C2C12 myoblasts were transfected with a miRNA inhibitor negative control (-ve control) or miR-351-3p inhibitor and after 4 d differentiation into myotubes, were treated for another 48 h with DMSO vehicle or (**C**) oxaliplatin or (**D**) cisplatin and were then stained for myosin and DAPI (*left*) to enable quantification of myotube diameter (*right*; two-way ANOVA; ****$P < 0.0001$; n = 4, ± SEM). C2C12 myotubes treated without (control, Con) or with leucovorin (LV) or irinotecan (IR) were also: (**E**) stained for myosin and DAPI (*left*) to enable quantification of myotube diameter (*right*); or (**F**) taken for western blot analysis of phosphorylated and total ERK1/2, and total protein (E, F; one-way ANOVA; **$P < 0.01$; n = 12, ± SEM).

Table S1. Supporting Information

Table S2. Supporting Information

Conflict of interest

None declared.

References

1. Fearon K, Strasser F, Anker SD, Bosaeus I, Bruera E, Fainsinger RL, et al. Definition and classification of cancer cachexia: an international consensus. *Lancet Oncol* 2011;**12**:489–495.
2. Powers SK, Lynch GS, Murphy KT, Reid MB, Zijdewind I. Disease-induced skeletal muscle atrophy and fatigue. *Med Sci Sports Exerc* 2016;**48**:2307–2319.
3. Tisdale MJ. Cachexia in cancer patients. *Nat Rev Cancer* 2002;**2**:862–871.
4. Martin L, Senesse P, Gioulbasanis I, Antoun S, Bozzetti F, Deans C, et al. Diagnostic criteria for the classification of cancer-associated weight loss. *J Clin Oncol* 2015;**33**:90–99.
5. Renfro LA, Loupakis F, Adams RA, Seymour MT, Heinemann V, Schmoll HJ, et al. Body mass index is prognostic in metastatic colorectal cancer: pooled analysis of patients from first-line clinical trials in the ARCAD database. *J Clin Oncol* 2016;**34**:144–150.
6. Sun L, Quan XQ, Yu S. An epidemiological survey of cachexia in advanced cancer patients and analysis on its diagnostic and treatment status. *Nutr Cancer* 2015;**67**:1056–1062.
7. Blum D, Stene GB, Solheim TS, Fayers P, Hjermstad MJ, Baracos VE, et al. Validation of the Consensus-Definition for Cancer Cachexia and evaluation of a classification model—a study based on data from an international multicentre project (EPCRC-CSA). *Ann Oncol* 2014;**25**:1635–1642.
8. O'Donoghue N, Shrotriya S, Aktas A, Hullihen B, Ayvaz S, Estfan B, et al. Clinical significance of weight changes at diagnosis in solid tumours. *Support Care Cancer* 2019;**27**:2725–2733.
9. Dewys WD, Begg C, Lavin PT, Band PR, Bennett JM, Bertino JR, et al. Prognostic effect of weight loss prior to chemotherapy in cancer patients. Eastern Cooperative Oncology Group. *Am J Med* 1980;**69**:491–497.
10. Prado CM, Baracos VE, McCargar LJ, Reiman T, Mourtzakis M, Tonkin K, et al. Sarcopenia as a determinant of chemotherapy toxicity and time to tumor progression in metastatic breast cancer patients receiving capecitabine treatment. *Clin Cancer Res* 2009;**15**:2920–2926.
11. Barret M, Antoun S, Dalban C, Malka D, Mansourbakht T, Zaanan A, et al. Sarcopenia is linked to treatment toxicity in patients with metastatic colorectal cancer. *Nutr Cancer* 2014;**66**:583–589.
12. Gilliam LA, St Clair DK. Chemotherapy-induced weakness and fatigue in skeletal muscle: the role of oxidative stress. *Antioxid Redox Signal* 2011;**15**:2543–2563.
13. Kimura M, Naito T, Kenmotsu H, Taira T, Wakuda K, Oyakawa T, et al. Prognostic impact of cancer cachexia in patients with advanced non-small cell lung cancer. *Support Care Cancer* 2015;**23**:1699–1708.
14. Barreto R, Mandili G, Witzmann FA, Novelli F, Zimmers TA, Bonetto A. Cancer and chemotherapy contribute to muscle loss by activating common signaling pathways. *Front Physiol* 2016;**7**:472.
15. Barreto R, Waning DL, Gao H, Liu Y, Zimmers TA, Bonetto A. Chemotherapy-related cachexia is associated with mitochondrial depletion and the activation of ERK1/2 and p38 MAPKs. *Oncotarget* 2016;**7**:43442–43460.
16. Damrauer JS, Stadler ME, Acharyya S, Baldwin AS, Couch ME, Guttridge D. Chemotherapy-induced muscle wasting: association with NF-κB and cancer cachexia. *Basic Appl Myol* 2008;**18**:139–148.
17. Alexander MS, Kunkel LM. Skeletal muscle microRNAs: their diagnostic and therapeutic potential in human muscle diseases. *J Neuromuscul Dis* 2015;**2**:1–11.
18. Zacharewicz E, Kalanon M, Murphy RM, Russell AP, Lamon S. MicroRNA-99b-5p downregulates protein synthesis in human primary myotubes. *Am J Physiol Cell Physiol* 2020;**319**:C432–C440.
19. Lee DE, Brown JL, Rosa-Caldwell ME, Blackwell TA, Perry RA Jr, Brown LA, et al. Cancer cachexia-induced muscle atrophy: evidence for alterations in microRNAs important for muscle size. *Physiol Genomics* 2017;**49**:253–260.
20. Freire PP, Fernandez GJ, Cury SS, de Moraes D, Oliveira JS, de Oliveira G, et al. The pathway to cancer cachexia: microRNA-regulated networks in muscle wasting based on integrative meta-analysis. *Int J Mol Sci* 2019;**20**:1962.
21. Chen R, Lei S, Jiang T, She Y, Shi H. Regulation of skeletal muscle atrophy in cachexia by microRNAs and long non-coding RNAs. *Front Cell Dev Biol* 2020;**8**:577010.
22. Lamon S, Zacharewicz E, Butchart LC, Orellana L, Mikovic J, Grounds MD, et al. MicroRNA expression patterns in post-natal mouse skeletal muscle development. *BMC Genomics* 2017;**18**:52.
23. Moraes LN, Fernandez GJ, Vechetti-Junior IJ, Freire PP, Souza RWA, Villacis RAR, et al. Integration of miRNA and mRNA expression profiles reveals microRNA-regulated networks during muscle wasting in cardiac cachexia. *Sci Rep* 2017;**7**:6998.
24. Bernardo BC, Ooi JY, Lin RC, McMullen JR. miRNA therapeutics: a new class of drugs with potential therapeutic applications in the heart. *Future Med Chem* 2015;**7**:1771–1792.
25. Murphy KT, Chee A, Trieu J, Naim T, Lynch GS. Importance of functional and metabolic impairments in the characterization of the C-26 murine model of cancer cachexia. *Dis Model Mech* 2012;**5**:533–545.
26. Van Laar JA, Rustum YM, der Wilt CLV, Smid K, Kuiper CM, Pinedo HM, et al. Tumor size and origin determine the antitumor activity of cisplatin or 5-fluorouracil and its modulation by leucovorin in murine colon carcinomas. *Cancer Chemother Pharmacol* 1996;**39**:79–89.
27. Williams GR, Deal AM, Shachar SS, Walko CM, Patel JN, O'Neil B, et al. The impact of skeletal muscle on the pharmacokinetics and toxicity of 5-fluorouracil in colorectal cancer. *Cancer Chemother Pharmacol* 2018;**81**:413–417.
28. Blankinship MJ, Gregorevic P, Allen JM, Harper SQ, Harper H, Halbert CL, et al. Efficient transduction of skeletal muscle using vectors based on adeno-associated virus serotype 6. *Mol Ther* 2004;**10**:671–678.

29. Thakur SS, James JL, Cranna NJ, Chhen VL, Swiderski K, Ryall JG, et al. Expression and localization of heat-shock proteins during skeletal muscle cell proliferation and differentiation and the impact of heat stress. *Cell Stress Chaperones* 2019;**24**: 749–761.
30. Murphy KT, Hossain MI, Swiderski K, Chee A, Naim T, Trieu J, et al. Mas receptor activation slows tumor growth and attenuates muscle wasting in cancer. *Cancer Res* 2019;**79**:706–719.
31. Murphy KT, Chee A, Gleeson BG, Naim T, Swiderski K, Koopman R, et al. Antibody-directed myostatin inhibition enhances muscle mass and function in tumor-bearing mice. *Am J Physiol Regul Integr Comp Physiol* 2011;**301**:R716–R726.
32. Acunzo M, Croce CM. MicroRNA in cancer and cachexia—a mini-review. *J Infect Dis* 2015;**212**:S74–S77.
33. Narasimhan A, Ghosh S, Stretch C, Greiner R, Bathe OF, Baracos V, et al. Small RNAome profiling from human skeletal muscle: novel miRNAs and their targets associated with cancer cachexia. *J Cachexia Sarcopenia Muscle* 2017;**8**: 405–416.
34. Vainshtein A, Sandri M. Signaling pathways that control muscle mass. *Int J Mol Sci* 2020;**21**:4759.
35. Murphy KT. The pathogenesis and treatment of cardiac atrophy in cancer cachexia. *Am J Physiol Heart Circ Physiol* 2016;**310**: H466–H477.
36. Pai VB, Nahata MC. Cardiotoxicity of chemotherapeutic agents: incidence, treatment and prevention. *Drug Saf* 2000;**22**:263–302.
37. O'Connell TM, Pin F, Couch ME, Bonetto A. Treatment with soluble activin receptor type IIB alters metabolic response in chemotherapy-induced cachexia. *Cancers (Basel)* 2019;**11**:1222.
38. Sirago G, Conte E, Fracasso F, Cormio A, Fehrentz JA, Martinez J, et al. Growth hormone secretagogues hexarelin and JMV2894 protect skeletal muscle from mitochondrial damages in a rat model of cisplatin-induced cachexia. *Sci Rep* 2017;**7**:13017.
39. Sorensen JC, Petersen AC, Timpani CA, Campelj DG, Cook J, Trewin AJ, et al. BGP-15 protects against oxaliplatin-induced skeletal myopathy and mitochondrial reactive oxygen species production in mice. *Front Pharmacol* 2017;**8**:137.
40. Nissinen TA, Degerman J, Rasanen M, Poikonen AR, Koskinen S, Mervaala E, et al. Systemic blockade of ACVR2B ligands prevents chemotherapy-induced muscle wasting by restoring muscle protein synthesis without affecting oxidative capacity or atrogenes. *Sci Rep* 2016;**6**:32695.
41. Braun TP, Szumowski M, Levasseur PR, Grossberg AJ, Zhu X, Agarwal A, et al. Muscle atrophy in response to cytotoxic chemotherapy is dependent on intact glucocorticoid signaling in skeletal muscle. *PLoS One* 2014;**9**:e106489.
42. Pin F, Barreto R, Couch ME, Bonetto A, O'Connell TM. Cachexia induced by cancer and chemotherapy yield distinct perturbations to energy metabolism. *J Cachexia Sarcopenia Muscle* 2019;**10**:140–154.
43. Shi H, Scheffler JM, Zeng C, Pleitner JM, Hannon KM, Grant AL, et al. Mitogen-activated protein kinase signaling is necessary for the maintenance of skeletal muscle mass. *Am J Physiol Cell Physiol* 2009;**296**: C1040–C1048.
44. Shi H, Scheffler JM, Pleitner JM, Zeng C, Park S, Hannon KM, et al. Modulation of skeletal muscle fiber type by mitogen-activated protein kinase signaling. *FASEB J* 2008;**22**:2990–3000.
45. Penna F, Costamagna D, Fanzani A, Bonelli G, Baccino FM, Costelli P. Muscle wasting and impaired myogenesis in tumor bearing mice are prevented by ERK inhibition. *PLoS One* 2010;**5**:e13604.
46. Quan-Jun Y, Yan H, Yong-Long H, Li-Li W, Jie L, Jin-Lu H, et al. Selumetinib attenuates skeletal muscle wasting in murine cachexia model through ERK inhibition and AKT activation. *Mol Cancer Ther* 2017;**16**:334–343.
47. Brown JL, Lee DE, Rosa-Caldwell ME, Brown LA, Perry RA, Haynie WS, et al. Protein imbalance in the development of skeletal muscle wasting in tumour-bearing mice. *J Cachexia Sarcopenia Muscle* 2018;**9**:987–1002.
48. Xie SJ, Li JH, Chen HF, Tan YY, Liu SR, Zhang Y, et al. Inhibition of the JNK/MAPK signaling pathway by myogenesis-associated miRNAs is required for skeletal muscle development. *Cell Death Differ* 2018;**25**: 1581–1597.
49. Baumann V, Winkler J. miRNA-based therapies: strategies and delivery platforms for oligonucleotide and non-oligonucleotide agents. *Future Med Chem* 2014;**6**: 1967–1984.
50. Wang JK, Wang Z, Li G. MicroRNA-125 in immunity and cancer. *Cancer Lett* 2019;**454**:134–145.